Interplay between competing exchange interactions and magnetocrystalline anisotropies in YFe_xMn_{12-x}: The magnetic phase diagram

C. Piqué,[1,*] E. Abad,[1] J. A. Blanco,[1] R. Burriel,[2] and M. T. Fernández-Díaz[3]
[1]*Departamento de Física, Universidad de Oviedo, 33007 Oviedo, Spain*
[2]*Instituto de Ciencia de Materiales de Aragón (CSIC-Universidad de Zaragoza), 50009 Zaragoza, Spain*
[3]*Institut Laue-Langevin, 38042 Grenoble, France*
(Received 21 September 2004; revised manuscript received 22 February 2005; published 25 May 2005)

The magnetic properties of tetragonal YFe_xMn_{12-x} compounds, which crystallize in the $ThMn_{12}$-type structure, are governed by both strong competing exchange interactions between the magnetic moments on three nonequivalent sites 8*i*, 8*j*, and 8*f* occupied by Mn (Fe) atoms preferentially in 8*i* (8*f*) and Mn-planar (Fe-axial) magnetocrystalline anisotropies. Using low field ac magnetic susceptibility versus temperature, zero-field-cooled and field-cooled magnetization versus temperature, and applied magnetic field, specific heat, x-ray-absorption spectroscopy at Fe *K* and Mn *K* edges, and neutron-diffraction experiments, the magnetic phase diagram of YFe_xMn_{12-x} has been determined. Up to six different phases were found as a function of the Fe concentration *x*. Some of them have not been thoroughly investigated until now. In particular, the antiferromagnetic ordering of the itinerant YMn_{12} is different from the phase proposed before, and the spin-glass-like phase observed at low temperatures for $2 \leqslant x \leqslant 6$ has been characterized in more detail. Contrary to other intermetallic Mn-based systems, the magnetism in YFe_xMn_{12-x} cannot be correlated in a straightforward way to 3*d*-3*d* distances and it seems to be more sensitive to the electronic density and the localization-delocalization of electronic band states on the three sites 8*i*, 8*j*, and 8*f*.

DOI: 10.1103/PhysRevB.71.174422 PACS number(s): 75.40.Cx, 75.25.+z, 75.50.Ee

I. INTRODUCTION

The magnetic properties of ternary intermetallic RFe_xM_{12-x} compounds, where *R* is a rare earth and *M* a stabilizing element (Al, Si, Ti, V, Mo, Sc, W, Ta), with the $ThMn_{12}$-type structure, have been studied intensively, mainly because the compounds with higher Fe content, such as $SmFe_{10}Si_2$, have permanent magnet properties.[1] Less work has been devoted to investigate these ternary compounds with low Fe concentration and when *M* is also a magnetic atom (Mn, Cr, or Co). Competing magnetocrystalline anisotropies and exchange interactions [ferromagnetic (F) or antiferromagnetic (AF) with itinerant or localized character] between the three magnetic elements in RFe_xM_{12-x} led to novel and interesting magnetic properties with different phases depending on the relative strength of the interaction parameters.

Mn compounds have rarely been reported as potential materials for producing high magnetization, but isolated Mn atoms exhibit magnetic moments of $5\mu_B$, which is larger than that of Fe. In particular, for an expanded crystal structure, Mn compounds might exhibit ferromagnetic behavior like in hexagonal $GdMn_6Ge_6$ and RMn_6Sn_6 (R = Tb, Ho, Gd, Dy) compounds.[2,3] Furthermore, sufficiently strong internal or external fields can break the AF ordering of Mn. For these materials, we cannot predict the behavior of Mn ternary compounds from their properties in the limiting concentration cases of binary compounds. In particular, Y_6Mn_{23} and Y_6Fe_{23} order magnetically at temperatures close to 500 K, while the ternary $Y_6Fe_xMn_{23-x}$ compounds show no evidence of long-range magnetic order for $4.6 < x < 13.8$ and a cluster glasslike state is also observed at low temperatures as a result of spin fluctuations.[4] In other compounds, as in the cubic Laves-phase YMn_2, the magnitude of the magnetic moment of Mn and its itinerant or localized character depends strongly on the Mn—Mn distances: above a critical spacing (2.667 Å), the Mn atoms are localized with a large magnetic moment, whereas below this critical value the Mn atoms have no intrinsic localized magnetic moment. Hence, in YFe_xMn_{2-x} the Fe- and Mn-rich compounds order magnetically while for $0.12 < x < 0.16$ a spin-glass state is found.[5]

Mn is the unique 3*d* magnetic element that stabilizes the tetragonal $ThMn_{12}$-type structure (space group $I4/mmm$). In this structure, there is a unique site for the Th atom (site 2*a*) and three sites (8*i*, 8*j*, and 8*f*) allowed for the 3*d* element. Below $T_N = 120$ K, YMn_{12} orders in a noncollinear AF arrangement with the magnetic moments in the basal plane of the tetragonal structure.[6] The Mn magnetic moments were found to be much reduced in comparison with other Mn alloys. The substitution of Fe for Mn leads to a preferential occupation of the sites 8*f* by Fe and the sites 8*i* by Mn, while the sites 8*j* are occupied by both Mn and Fe.[7] The compounds with low Fe concentration ($x < 7$) are AF, but, in contrast to the $Y(Fe,Mn)_2$ and $Y_6(Fe,Mn)_{23}$ systems, the substitution of Fe for Mn leads to an increase of both the ordering temperature T_N and the magnitude of magnetic moments, at least in the sites 8*i* and 8*j*, reaching a maximum at around $x = 5$.[8] The YFe_8Mn_4 compound is F ($T_C = 250$ K) with the magnetic moments aligned along the *c* axis, while below 150 K the AF structure found for the AF compounds appears superimposed.[9] However, recent results[10] show still some discrepancies regarding the magnetic structure and the nature of phase transitions in these YFe_xMn_{12-x} compounds. This work proposes a ferromagnetic ordering from $x \geqslant 6$ and no AF transition at low temperatures for these F materials. In

TABLE I. Refinement parameters of YFe_xMn_{12-x} found at room temperature: x_{ref} is the refined Fe composition; a and c are the lattice parameters. Shown are the distribution of the Fe content on the three transition-metal sites 8i, 8j, and 8f; the fractional position coordinates; the nearest-neighbor distances between the three sites 8i, 8j, and 8f; and the reliability R_B^N factor.

		%Fe			Coordinates		Lattice parameters		Distance (Å)			
	x_{ref}	8i	8j	8f	x (8i)	x (8j)	a (Å)	c (Å)	8i-8i	8j-8f	8f-8f	R_B^N (%)
YMn_{12}					0.362(1)	0.279(1)	8.5421(5)	4.7280(3)	2.36	2.45	2.36	5.2
YFe_2Mn_{10}	2.1(1)	3.6(4)	16.4(4)	33.4(4)	0.356(1)	0.258(1)	8.5366(5)	4.7503(5)	2.38	2.44	2.37	4.1
YFe_4Mn_8	4.2(1)	9.2(3)	37.0(2)	59.0(3)	0.364(1)	0.272(2)	8.529(1)	4.7603(5)	2.31	2.45	2.38	5.6
YFe_6Mn_6	6.3(3)	18.4(3)	59.8(5)	78.2(5)	0.362(3)	0.276(1)	8.4988(9)	4.7588(3)	2.35	2.44	2.38	4.5
YFe_8Mn_4	8.2(1)	38.4(4)	77.2(4)	88.8(4)	0.363(3)	0.280(1)	8.473(1)	4.7650(5)	2.32	2.44	2.38	4.0

addition, a spin-glass-like behavior has been observed in these series for all the compositions. Recently, complementary works have also been reported on the electrical resistivity of polycrystalline RFe_xMn_{12-x} compounds with $0 \leqslant x \leqslant 9$ over the temperature range 4–400 K.[11,12] It follows from these works that the anomalous rise of the electrical resistivity for $x=0$, below T_N, is explained invoking electron scattering by substitutional and thermal spin disorder in addition to scattering by phonons and impurities, instead of using the theory of Elliot and Wedgood[13] for magnetic superzones.[14]

In this paper, we focus our attention in YFe_xMn_{12-x}, as a first step to study the compounds with a magnetic rare earth, in the hope of getting better insight into the main interactions that govern the physics of the system, i.e., the magnetocrystalline anisotropies and the exchange interactions in the 3d sublattices. In particular, to understand the role of localization-delocalization effects on the 3d magnetic moment, the magnetic phase transitions previously observed, and the spin-glass behavior, we have measured magnetization, ac susceptibility, heat capacity, neutron diffraction, and x-ray-absorption spectroscopy in YFe_xMn_{12-x} ($x=0,2,4,6,8$). Using all this information, the magnetic phase diagram of YFe_xMn_{12-x} has been established.

This paper is organized as follows. Section II is devoted to the experimental details. The results and discussion about the structural properties, macroscopic magnetic properties, and the magnetic structures obtained from neutron-diffraction experiments are given in Sec. III. The magnetic phase diagram and the main results are presented in Sec. IV, while a general conclusion is summarized in Sec. V.

II. EXPERIMENTAL DETAILS

Polycrystalline samples of composition YFe_xMn_{12-x} ($x=0,2,4,6,8$) have been synthesized by induction melting of the constituent elements with an excess of Mn due to the high Mn vapor pressure. They were subsequently annealed at 1000 °C for 5 days in argon atmosphere. The samples were then checked by x-ray powder diffraction, in a high-resolution SEIFERT-XRD-3000 diffractometer at the University of Oviedo, for phase purity. For YMn_{12}, some small amounts of Y_6Mn_{23} (less than 2%) and β-Mn (11%) were detected as in the work of Morales *et al.*[9] For the other YFe_xMn_{12-x} compounds ($x=2,4,6,8$), the $Y_6(FeMn)_{23}$ phase was not present and the amount of β-Mn was getting smaller with the rising of the Fe concentration, being 5% for $x=2$ and almost zero for $x \geqslant 4$.

The dc magnetization and ac susceptibility were measured in a Quantum Design SQUID magnetometer at the University of Zaragoza and the University of País Vasco. The zero-field-cooled (ZFC) isofield magnetization $M(T)$ was measured at the desired magnetic field during heating. The field-cooled (FC) $M(T)$ behavior was measured on heating at a fixed field, after cooling the sample from the paramagnetic phase. In some cases, we have also measured $M(T)$ in a field cooled during the cooling process from room temperature.

The heat capacity $C_p(T)$ was measured in an adiabatic calorimeter based on the heat pulse method at the University of Oviedo. For all the compounds studied, the sample mass used for the measurements was around 3 g. The accuracy of the equipment is 0.3% for temperatures higher than 100 K and better than 1.5% for the lowest temperatures.[15] The neutron-diffraction spectra were collected using the D1B diffractometer at the ILL (Grenoble, France). Rietveld refinements were carried out using the FULLPROF program.[16] Finally, x-ray-absorption spectra were recorded at the beam line 7.1 at SRS (Daresbury), working in the usual transmission geometry.

III. RESULTS AND DISCUSSION

A. Structural properties

All the YFe_xMn_{12-x} ($x=0,2,4,6,8$) samples were found to crystallize in the body-centered-tetragonal structure ($ThMn_{12}$-type) having $I4/mmm$ space group. The Y atoms lay at the Wyckoff position 2a and the transition metals at positions 8i, 8j, and 8f. The site occupancies, refined from the neutron-diffraction patterns collected at room temperature, show that Fe prefers to occupy the sites 8f whereas Mn are found preferentially on the sites 8i, in good agreement with the results found previously by other authors.[7,9] The main crystallographic data of the investigated YFe_xMn_{12-x} compounds are gathered in Table I. The cell parameter a decreases linearly with the Fe concentration, while c remains nearly constant. Within the accuracy of the experiment, the structural parameters are temperature-independent except for the cell parameters. Although a and c decrease linearly from

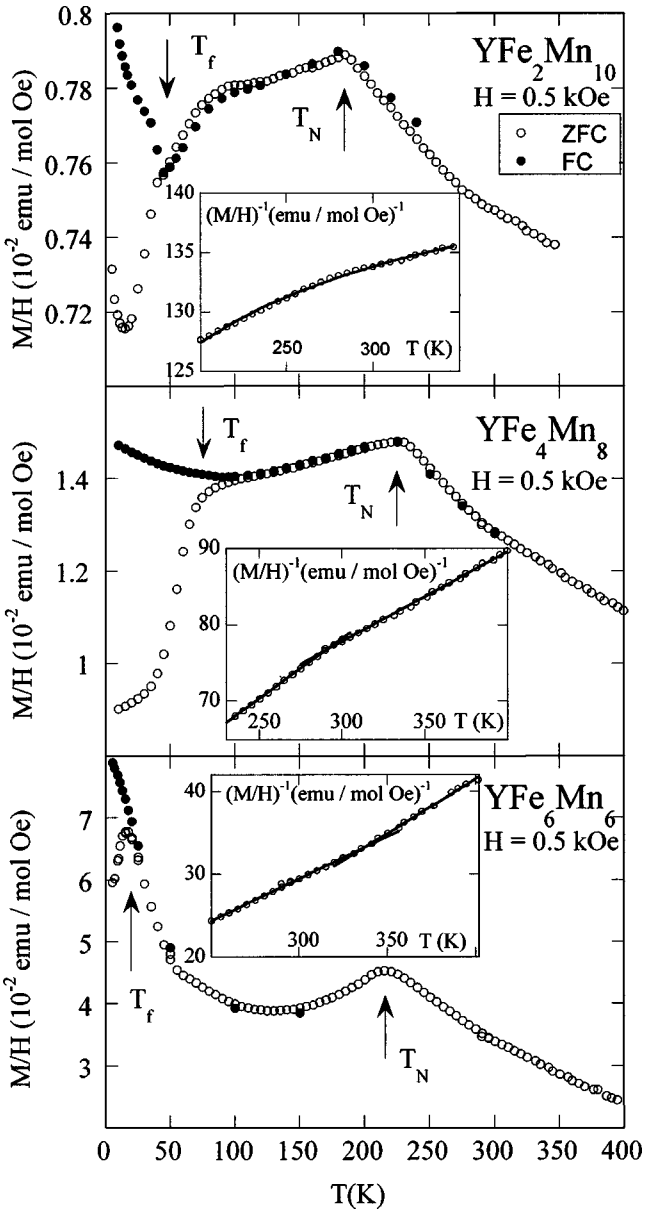

FIG. 1. Temperature dependence of the dc susceptibility for YFe_xMn_{12-x} ($x=2,4,6$) in ZFC and FC conditions, under an applied field of 0.5 kOe. T_N is the Néel temperature and T_f the spin-freezing temperature. The insets show the temperature dependence of the inverse susceptibility in the paramagnetic region. The solid line in the inset of $x=2$ represents the fit to a modified Curie-Weiss law: $\chi=\chi_0+C/(T-\theta_p)$. For $x=4$ and $x=6$, a Curie-Weiss law with a change of slope is more likely.

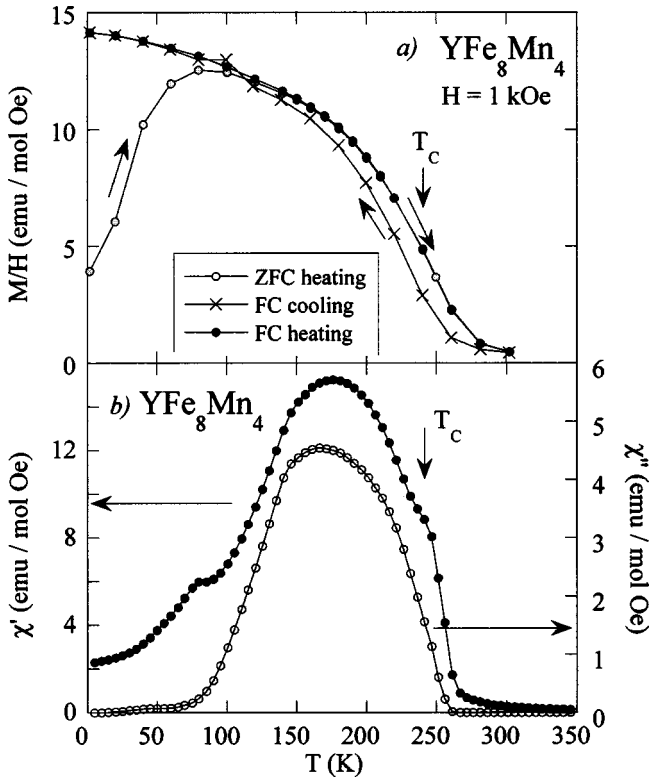

FIG. 2. Temperature dependence of the dc and ac susceptibility for YFe_8Mn_4. The dc susceptibility (a) has been measured in ZFC and FC conditions, under an applied field of 1 kOe. T_C is the Curie temperature. Hysteresis is observed in the FC data between the points measured on cooling and heating. Temperature dependence of the real (●) and imaginary (○) parts of the ac magnetic susceptibility (b), measured under an ac field of 4.5 Oe at 10 Hz. The lines are guides for the eye.

room temperature, below 50 K they are almost constant, with a similar trend to the one found from the thermal expansion measured on $TbFe_6Mn_6$.[17] This behavior at low temperatures suggests that the volume magnetostriction is positive and of such magnitude that it fully cancels the lattice thermal expansion.

In order to get a better insight into the discussion of the magnetic structures in YFe_xMn_{12-x} (see below), a detailed analysis of the 3*d*-3*d* interatomic distances has been made (see Table I). The nearest 3*d* atoms correspond to positions 8*i*-8*i*, though these distances are similar to the corresponding distances of atoms at positions 8*f*-8*f*. Neither these values nor the mean interatomic distances between a 3*d* crystallographic site and its nearest neighbors vary with the Fe concentration through the YFe_xMn_{12-x} series investigated.

B. Magnetic properties

In order to make a macroscopic magnetic characterization of the YFe_xMn_{12-x}, we have performed susceptibility and magnetization measurements. The temperature dependences of the dc susceptibility M/H for YFe_xMn_{12-x} under applied fields of 0.5 kOe (for $x=2,4,6$) and 1 kOe (for $x=8$), measured in ZFC and FC conditions, are shown in Figs. 1 and 2(a), respectively. For the higher Fe concentration $x=8$, the susceptibility is three orders of magnitude larger than that found for the lowest Fe concentrations $x=2$ and 4, and has a stronger temperature variation when x increases. The measured susceptibilities confirm that the compound with $x=8$ is F, the one with $x=6$ is AF, and the compounds with $x=2$ and 4 are itinerant AF, as described in a previous report.[9] The small amount of the ferrimagnetic impurity Y_6Mn_{23} ($T_C=486$ K) is sufficient to disguise the magnetic measurements for YMn_{12}.

In Fig. 1, besides the AF ordering observed at the Néel temperature ($T_N=185\pm5$ K, 225 ± 5 K, and 215 ± 5 K for x

=2,4,6, respectively), a second anomaly is found at lower temperatures, below which the magnetic data differ in the ZFC and FC measurements. This behavior seems to be related to the spin-glass phase previously observed for all compositions.[10] From the ZFC and FC variations, we can estimate the freezing temperatures to be at around $T_f = 45\pm5$ K, 75 ± 5 K, and 20 ± 5 K for $x=2,4,6$, respectively.

On the other hand, in the paramagnetic region the temperature dependence of the inverse susceptibility $(M/H)^{-1}$ does not vary linearly with the temperature for $x=2$ [see the inset in Fig. 1(a)]. A modified Curie-Weiss expression[18] accounting for the contribution of conduction electrons to the magnetic susceptibility, χ_0, needs to be used for fitting the experimental data, $\chi=\chi_0+C/(T-\theta_p)$ yielding to the values $\chi_0=6.84\times10^{-3}$ emu/mol Oe, $\theta_p=20$ K, and from the Curie constant we obtain the average magnetic moment per $3d$ atom $\mu_{\text{eff}}=0.34\ \mu_B$/at. In contrast, for $x=4$ and $x=6$, $(M/H)^{-1}$ shows a change of slope [see the insets in Figs. 1(b) and 1(c)]. The paramagnetic Curie temperature and the effective magnetic moments obtained below and above this slope change are as follows for the $x=4$ compound, $\theta_p=-198$ K and $\mu_{\text{eff}}=2.1\ \mu_B$/at (below), $\theta_p=-360$ K and $\mu_{\text{eff}}=2.4\ \mu_B$/at (above); and for the $x=6$ compound, $\theta_p=-11$ K and $\mu_{\text{eff}}=2.6\ \mu_B$/at (below), $\theta_p=-85$ K and $\mu_{\text{eff}}=2.2\ \mu_B$/at (above). This behavior in the paramagnetic phase could indicate the existence of short-range interactions enhanced by spin fluctuations, as suggest similar phenomena observed in $Tb(FeMn)_2$ compounds.[19] It is worth noting the following two main results found on YFe_8Mn_4 and YFe_6Mn_6 compounds.

1. Zero-field-cooled and field-cooled $M(T)$ data irreversibility and anomalous ac susceptibility in YFe_8Mn_4

For $x=8$ (Fig. 2(a)) together with a rapid increase in M/H below $T_C=250\pm10$ K, there are differences between the ZFC and FC measurements below 100 K. As shown from neutron-diffraction measurements (see Sec. III D), for $T<T_t=150$ K a change in the magnetic structure takes place leading to the appearance of an AF component and resulting in an effective canted magnetic structure. The lower value of M in the ZFC curve for this compound could be explained as an intrinsic pinning of the F components by the anisotropy of this AF component, as it was proposed in $Nd_{1-x}Dy_xMn_2Ge_2$.[20]

In Fig. 2(b), the ac susceptibility for the F compound $x=8$ exhibits two anomalies in χ', while only one is detected in χ''. A broad anomaly (extended through 100 K) is observed in both χ' and χ'' close to the Curie temperature. Below $T_t=150$ K, where an additional AF component appears, the susceptibility falls down. It could be due to a reduction in the degrees of freedom of the magnetic moments inhibiting the response to an applied ac magnetic field. Similar behaviors have been found in the 1:2 compounds $Tb(MnFe)_2$ and $Zr(FeCo)_2$.[19,21] In addition, there is a knee-like anomaly in χ' at around 90 K, where differences between FC and ZFC magnetization measurements have been observed. The temperature dependence of the inverse ac magnetic susceptibility of YFe_8Mn_4 above the Curie temperature follows a Curie-Weiss law. The calculated effective magnetic moment and paramagnetic Curie temperature are $\mu_{\text{eff}}=2.97\ \mu_B$/at and $\theta_p=253$ K. On the contrary, the inverse ac magnetic susceptibility for the $x=2$ compound in the paramagnetic region presents a curvature, and the one of $x=4$ shows a change of slope at about 300 K, in a way similar to the data observed in dc susceptibility measurements.

The isothermal magnetization curves of YFe_8Mn_4 show a ferromagneticlike behavior with a rapid increase at low fields, but no saturation is seen up to the highest applied field of 100 kOe. In this material, the anisotropy field, H_a, has been measured in an oriented powder sample, applying the magnetic field along and perpendicular to the c axis of the tetragonal structure. The easy magnetization axis turned out to be the c direction for all the temperatures measured (10–200 K). H_a is higher at low temperature, as was also observed in $YFe_{11}Ti$,[1] but the magnitude in our case is smaller ($H_a<10$ kOe at $T=10$ K for YFe_8Mn_4 compared to 40 kOe for $YFe_{11}Ti$).

2. Low-temperature spin-glass-like behavior in YFe_6Mn_6

The temperature dependence of the real and imaginary components of the ac magnetic susceptibility for YFe_6Mn_6 shows two peaks in both χ' and χ''; in contrast with the behavior of the compound with $x=8$, the one at higher temperature corresponds to the Néel temperature T_N and the second one is associated with the freezing temperature T_f, where FC and ZFC differences have been observed in χ_{dc} measurements. We ascribe this latter to spin-glass behavior, as was pointed out previously.[10] One of the important features in a spin-glass material,[22] which characterizes the random freezing of the magnetic moments, is the appearance of a cusp in the ac susceptibility at T_f, which depends both on magnetic field and frequency. As a trademark of this behavior found in YFe_xMn_{12-x} compounds, we present in Fig. 3 the frequency and magnetic field dependences of χ' for YFe_6Mn_6. The position of the maximum at around $T_f=20$ K shifts to higher temperatures with increasing frequency [see Fig. 3(a)] and the anomaly is strongly reduced by the application of 10 kOe [see Fig. 3(b)]. The relative variation of T_f per frequency decade, $\Delta T_f/(T_f\Delta \ln \omega)$, is about 24×10^{-3}, in agreement with the values typically reported for metallic spin glasses.[22] We have plotted in the inset of Fig. 3(a) the spin-freezing temperatures (defined as the cusp in the ac susceptibility) versus $1/\ln(\nu_0/\nu)$. From this figure, it can be seen that the slowing down of the dynamics follows a Vogel-Fulcher law.[22] In addition, initial magnetization curves measured in a YFe_6Mn_6 compound show a linear variation of the magnetization, with no metamagnetic transitions up to 70 kOe.

To summarize the data presented in Figs. 1–3, the magnetization and susceptibility measurements suggest the coexistence and competition of F and AF components in the magnetic structure of YFe_xMn_{12-x} compounds. In particular, for the AF compounds $2\leqslant x\leqslant 6$ ($T_N\sim200$ K), a spin-glass-like phase is favored below $\sim$80 K, while for the F compound $x=8$ ($T_C\sim250$ K) an AF component develops below $T_t=150$ K. In the following, we shall concentrate on the nature of the magnetic phases observed in these materials from a heat capacity study.

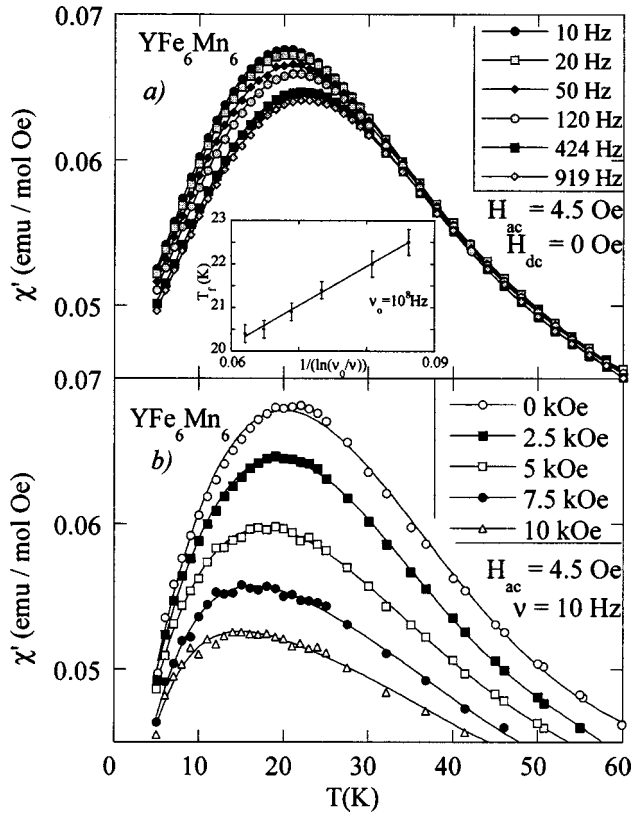

FIG. 3. Temperature dependence of the real part of the ac magnetic susceptibility for YFe_6Mn_6 for different frequencies (a) and dc magnetic fields (b). The line is a polynomial fit.

C. Heat-capacity measurements

The heat-capacity (C_p) measurements of YFe_xMn_{12-x} ($x=0,2,4,6,8$) are shown in Fig. 4. For all the compounds, except for the one with the highest Fe concentration $x=8$, we observe a second-order anomaly corresponding to the AF ordering of the 3*d* sublattice. The anomalies are very reduced and smoothed owing to the itinerancy of the 3*d* electrons. Taking the Néel temperature at the maximum of the C_p anomaly, we obtain $T_N=110\pm3$ K ($x=0$), $T_N=181\pm3$ K ($x=2$), $T_N=224\pm3$ K ($x=4$), and $T_N=215\pm3$ K ($x=6$), which are quite close to those found in magnetic and neutron measurements (see below). In the ferromagnetic compound, $x=8$, the anomaly appears to be very much extended in temperature, and only a very small change of slope at $T_C=242\pm3$ K is observed (see the inset of Fig. 4). This could be due to the substitutional disorder of the Fe/Mn atoms and broad contributions due to the appearance of an AF component at 150 K that leads to a progressive canting of the magnetic moments.

In order to evaluate the magnetic contribution to the total heat capacity, we have taken the heat capacity of $LuFe_{11}Ti$ as the baseline that includes phonon and electronic contributions up to 300 K. This compound has been successfully used as a baseline to study the spin reorientation transition of $NdFe_{11}Ti$.[23] Furthermore, $LuFe_{11}Ti$ has a Debye temperature $\theta_D=371$ K and an electronic contribution $\gamma=146$ mJ/mol K^2, calculated from the low-temperature data,

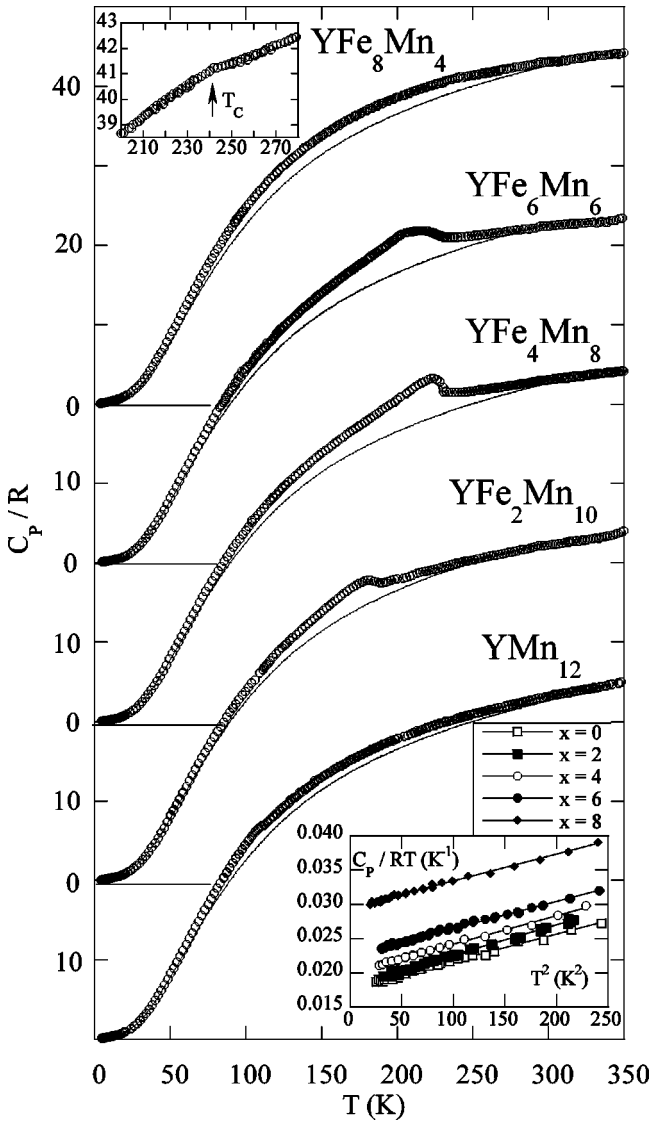

FIG. 4. Heat-capacity measurements of YFe_xMn_{12-x} ($x=0,2,4,6,8$) with the nonmagnetic base line (solid line). The inset 1 shows the change of slope at T_C for YFe_8Mn_4. In inset 2, the low-temperature heat-capacity measurements showing the linear fit (line) to the expression $C/T=\gamma+\beta T^2$ are presented.

similar to the values found in our compounds, and there are experimental and theoretical evidences that the magnetic contribution to the heat capacity in 3*d* metals is very small at temperatures below one-half the magnetic ordering temperature.[24] In Fig. 4, we present, as a continuous line, the heat capacity of $LuFe_{11}Ti$ from 5 to 300 K.[23] From the subtraction of this baseline, the resulting contribution of the magnetic ordering in YFe_xMn_{12-x} ($x=0,2,4,6,8$) is obtained and the relevant parameters are gathered in Table II.

The entropy content of the phase transition S_{mag} and the heat-capacity jump ΔC_{mag} at the ordering temperature are very reduced compared to the values obtained in a localized model [$S_{mag}=nR\ln(2S+1)=13.2R$ and $\Delta C_{mag}=24R$, where n is the number of magnetic atoms with spin S, and R is the ideal gas constant, and have been calculated for $S=1$].

The YMn_{12} binary alloy has the lowest value of the jump in the YFe_xMn_{12-x} series ($\Delta C_{mag}/3d$ atom$=0.04R$) and is

TABLE II. Transition temperatures in the YFe_xMn_{12-x} series: the Néel temperature (T_N) and the Curie temperature (T_C) have been obtained from heat-capacity measurements, the spin-freezing temperature (T_f) from magnetic measurements. Electronic specific-heat coefficient (γ), Debye temperature (θ_D), magnetic entropy content of the magnetic anomaly (ΔS_{mag}), and the jump of the specific-heat anomaly (ΔC_{mag}) at the ordering temperature in the compounds investigated.

	T_N (K)	T_C (K)	T_f (K)	γ (mJ/mol K^2)	θ_D (K)	ΔS_{mag}/R f.u.	ΔC_{mag}/R f.u.
YMn_{12}	110(3)			148(9)	426(3)	2.3	0.48
YFe_2Mn_{10}	181(3)		45(5)	151(9)	410(4)	2.3	3.17
YFe_4Mn_8	224(3)		75(5)	166.4(4)	419(1)	3.3	5.01
YFe_6Mn_6	215(3)		20(5)	186.9(4)	424(2)	3.3	4.62
$LuFe_6Mn_6$	216(3)			176.8(4)	412(2)	3.6	4.60
YFe_8Mn_4		242(3)		244.9(4)	426(1)	3.5	

also smaller than most of the intermetallic compounds, such as Tm_2Fe_{17} ($0.12R$),[25] $Y_2Fe_{14}B$ ($1.7R$),[26] and YMn_2 ($2.2R$),[27] but has the same order of magnitude as in the itinerant compound $ZrZn_2$ ($0.025R$).[28] From these results, we conclude that YMn_{12} is an itinerant AF with reduced magnetic moments and with important spin fluctuations above T_N that cause a contribution to the heat capacity. This main feature agrees with the interpretation of μSR experiments in YMn_{12}.[29]

One important issue of our results is the increase of ΔC_{mag} with the Fe concentration, reaching a maximum for $x=4$. This compound also has the highest value of Néel temperature. This feature means that there is an evolution from an itinerant ($x=0$) to a more localized behavior of the 3*d* electrons upon the addition of Fe in YFe_xMn_{12-x}. For $x=6$, both T_N and ΔC_{mag} diminish because of the proximity of the crossover point from AF to F ordering.

No additional anomalies have been observed in the low-temperature region confirming thereby that the features seen in magnetic measurements at low temperatures (see Sec. III B) do not arise from any long-range magnetic ordering. A spin-glass-like transition, with low heat-capacity contribution, is more likely. Spin glasses can show a linear term in the heat capacity in some temperature range below the freezing temperature.[22] Therefore, besides the electronic contribution, the random freezing of the magnetic moments in the alloys with $x=2,4,6$ can give an additional small contribution in the linear term of the heat capacity.

For obtaining information about the electronic specific heat coefficient γ the low-temperature heat-capacity data, C_p/T versus T^2, is shown as an inset in Fig. 4. It is worth noting that for $x=0$ and $x=2$, the β-Mn impurity, with no magnetic order but with a large value of γ(70 mJ/K^2 mol),[30] influences the results on YFe_xMn_{12-x}. For this reason, we have made a correction of the experimental values to subtract the contribution associated with β-Mn using the amounts obtained from diffraction data in these two samples. As we see in the figure, all the plots are linear, so the magnetic contribution in this temperature range is very small or has a T^3 dependence. The data were least-squares fitted to the expression, $C/T=\gamma+\beta T^2$, and the values of the electronic coefficient, γ and Debye temperatures, θ_D, derived from the fit are listed in Table II. The magnitude of γ per Mn atom ($\gamma=12$ mJ/K^2 at for YMn_{12}) is not large, compared to other Mn metallic systems with large spin fluctuations, such as Y(Sc)Mn_2 (70 mJ/K^2 at),[31] $LaMn_4Al_8$ (66 mJ/K^2 at).[32] In fact, this value for YMn_{12} is of the same order of magnitude as the values found in Lu_6Mn_{23} (12 mJ/K^2 at),[33] YMn_2 (7.5 mJ/K^2 at),[27] and YMn_4Al_8 (21 mJ/K^2 at).[32] This is in agreement with NMR (Ref. 34) and μSR (Ref. 29) results that found quasistatic Mn moments below T_N. The coefficient γ is typically an order of magnitude larger in 3*d* systems than in simple *s*-*p* metals due to the relatively narrower 3*d* band at the Fermi level ($LuZn_{12}$ with the same crystallographic structure has $\gamma=0.8$ mJ/K^2 Zn at).

To correlate the character of the magnetic order with the Fe content, *x*, the variation of the main parameters [jump of C_p at the transition temperature, ΔC_{mag}, electronic coefficient, γ magnetic moments at 3*d* sites, μ_{3d} (see the next section), and ordering temperature, T_{ord}] are presented in Fig. 5. The value of γ rises with the Fe concentration, as the magnetic moment, the jump of C_p, and T_{ord} do. This agrees with the prediction of rise in T_{ord} when the density of states at the Fermi level gets large for the itinerant electron model.[35] The highest value of the density of states at the Fermi level, $n(E_F)$, corresponds to the F compound YFe_8Mn_2, as expected.

Trying to obtain a deeper insight into the modification of the density of states linked to the substitution of Mn by Fe, we have performed an x-ray absorption spectroscopy study at the Fe *K* and Mn *K* edges at room temperature. The x-ray-absorption near-edge structure (XANES) region around the absorption threshold at the Mn *K* and Fe *K* edges for the YFe_xMn_{12-x} ($x=4,6,8$) compounds has been measured. The absorption edge position does not depend on the composition. As the Fe concentration increases, the peak located near the absorption threshold of Mn reduces. This behavior reflects a net decrease in the density of empty states near the Fermi level in the Mn 3*d* band; this band is progressively filled up by the Fe acting as an electron donor. The same conclusion can be drawn from the measurements at the Fe *K* edge. These results show that the change in the magnetic behavior is driven by the effects in the density of states produced by the additional electrons coming from Fe, rather than solely from the interatomic distances.

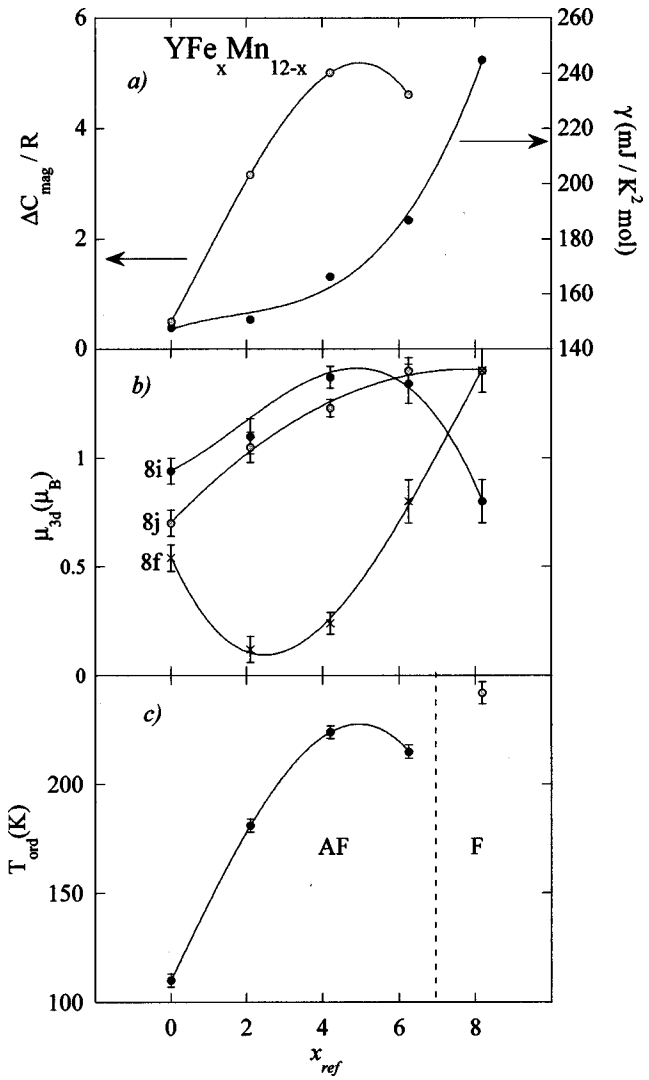

FIG. 5. Jump of the magnetic specific-heat anomaly (ΔC_{mag}) (○) and electronic specific-heat coefficient (γ) (●) of YFe_xMn_{12-x} (a); magnetic moment at the sites $8i$(●), $8j$(○), and $8f$(×), derived from neutron-scattering experiments (b); ordering temperature [● (T_N) and ○ (T_C)] from heat-capacity measurements (c), as functions of the neutron refined Fe content (x_{ref}).

D. Magnetic structure

From neutron-diffraction experiments, the magnetic structure and its evolution with temperature for the YFe_xMn_{12-x} ($x=0,2,4,6,8$) alloys have been determined. In Fig. 6, the neutron-diffraction spectrum at 1.5 K for the binary compound YMn_{12} is presented. The best agreement between calculated and observed intensities corresponds to a noncollinear AF structure of $3d$ moments in the basal plane. The propagation vector is $\mathbf{Q}=(1,0,0)$, which is located in the point M of the first Brillouin zone. The magnetic arrangement is described according to the representation Γ_3' for the three crystallographic sites $8i$, $8j$, and $8f$ [Γ_3':$(-A_{1xy}+A_{5xy})_{8i}+(A_{1xy}-A_{5xy})_{8j}+(-A_{1x}+A_{5x}+G_{1y}-G_{5y})_{8f}$], where $A_{1xy}=S_{1x}-S_{2x}-S_{3y}+S_{4y}$($A_{5xy}=S_{5x}-S_{6x}-S_{7y}+S_{8y}$), $A_{1x}=S_{1x}-S_{2x}-S_{3x}+S_{4x}$($A_{5x}=S_{5x}-S_{6x}-S_{7x}+S_{8x}$), and $G_{1y}=S_{1y}-S_{2y}+S_{3y}-S_{4y}$($G_{5y}=S_{5y}-S_{6y}+S_{7y}-S_{8y}$). The projection of the AF structure in the basal plane is seen in Fig. 7(a). This arrangement is different from the one proposed by Deportes[6] and Morales[9] because of the change in the orientation of the $8f$ moments. In addition, we observe that there is not any straightforward relation between the effective coupling F/AF and the interatomic distance between $3d$ atoms in these alloys. In fact, the two nearest $8i$-$8i$ Mn atoms have AF coupling but the nearest $8f$-$8f$ Mn ions situated at the same distance, (2.36 Å), have F coupling. The magnetic moment in the $8f$ site is the lowest (see Table III). Furthermore, the arrangement of the $8j$ sublattice moment can be explained by $8j$-$8f$ (2.45 Å) AF coupling. Other aspects like local environment or local density of states at the Fermi level seem to play a more important role than the distances between the $3d$ ions.

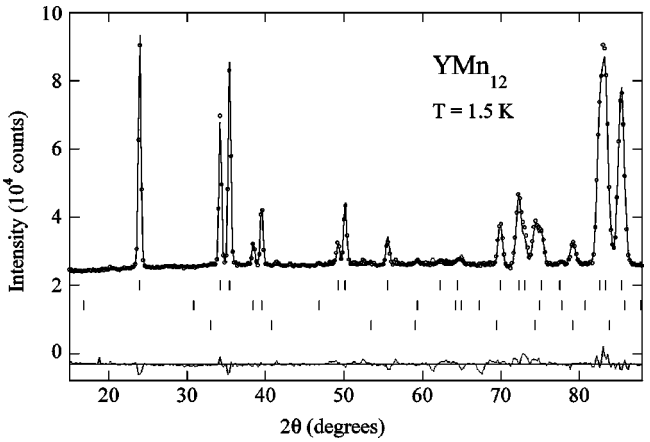

FIG. 6. Observed (points), Rietveld method fit (solid line), and difference (bottom) neutron-diffraction profiles for YMn_{12} measured at 1.5 K. The first, second, and third series of tick marks correspond to the positions of the allowed Bragg reflections: top, nuclear; middle, AF $3d$ component; bottom β-Mn impurity.

For the compounds with Fe concentrations $x=2$, 4, and 6, we have found the same magnetic mode associated with Γ_3' but with different sublattice relative arrangement. The orientation of the $8f$ magnetic moments in the com-

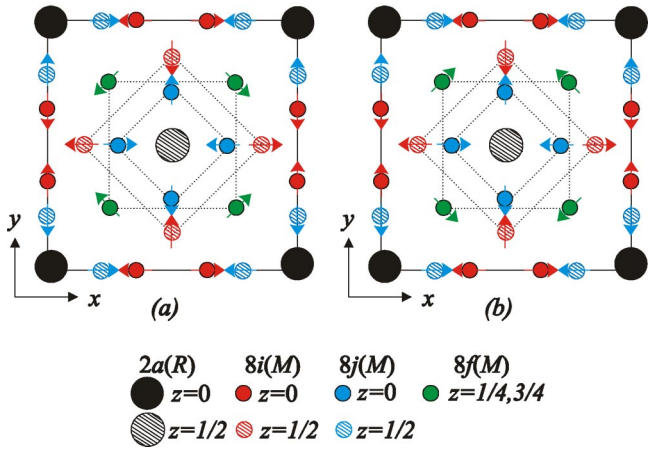

FIG. 7. Projected magnetic structure in the basal ab plane of YMn_{12} (a) and YFe_xMn_{12-x} ($x=2,4,6,8$) (b). Note the different arrangement for the magnetic moments at the site $8f$.

TABLE III. Magnetic parameters obtained from the neutron-diffraction profile refinements of YFe_xMn_{12-x}: Néel temperature (T_N); Curie temperature (T_C); transition temperature (T_t); magnetic moment in the sites 8*i*, 8*j*, and 8*f* (μ_{8i}, μ_{8j}, μ_{8f}); and reliability factors R_B^N and R_B^M.

	T_N (K)	T_C (K)	T_t (K)	μ_{8i} (μ_B)	μ_{8j} (μ_B)	μ_{8f} (μ_B)	R_B^N (%)	R_B^M (%)
YMn_{12}	115(5)			0.92(6)	0.64(5)	0.55(6)	5.8	8.5
YFe_2Mn_{10}	185(5)			1.10(8)	1.05(7)	0.12(6)	6.2	8.7
YFe_4Mn_8	230(5)			1.34(5)	1.24(4)	0.34(4)	5.5	4.6
YFe_6Mn_6	220(5)			1.34(9)	1.40(6)	0.8(1)	5.4	6.5
YFe_8Mn_4		250(5)	150(10)	0.8(1)	1.4(1)	1.4(1)	4.1	6.3

pounds with $x \geqslant 2$ is inverted with respect to the one found in YMn_{12} $[\Gamma_3': (-A_{1xy}+A_{5xy})_{8i}+(A_{1xy}-A_{5xy})_{8j}+(A_{1x}-A_{5x}-G_{1y}+G_{5y})_{8f}]$. This arrangement is the same as the one described previously for YMn_{12} by Deportes[6] and Morales.[9] The projection of this structure is presented in Fig. 7(b). These solutions are different because the addition of Fe in the 8*f* and 8*j* sites changes the relative orientation between the magnetic moments of the nearest 8*j*-8*f* atoms from effective antiparallel to parallel direction and the contrary for the 8*i*-8*f* atoms. This means that the interaction Mn—Mn is AF, the Fe—Fe is F, and the Mn—Fe is AF.

From the analysis of the neutron spectra of YFe_xMn_{12-x} at 1.5 K, the main refinement parameters are presented in Table III. As we see in Fig. 5, the magnetic moment associated with the site 8*f* for $x=0$ is $0.55\mu_B$, for $x=2$ (33% Fe in site 8*f*) is nearly zero, and for $x=4$ (59.2% Fe in site 8*f*) rises in the opposite direction. An AF coupling in this site between the Fe and the Mn ions can explain this feature, as it has been observed by x-ray magnetic circular dichroism measurements.[36] The magnitude of the magnetic moments in sites 8*i* and 8*j* increases with the addition of Fe, giving rise to an increase of T_N. This behavior is very different from the one observed in the series RFe_xMn_{2-x} and $R_6Fe_xMn_{23-x}$.[37,38] In the latest case, the addition of Fe causes the magnetic moment and T_{ord} to diminish with the disappearance of the long-range magnetic order for intermediate concentrations. This behavior is similar to the one found in the site 8*f* for YFe_2Mn_{10}.

The YFe_8Mn_4 magnetic structure at 1.5 K is canted showing a coexistence of F components $[\mathbf{Q}_1=(0,0,0)]$ along *c* and AF ones $[Q_2=(1,0,0)]$ in the basal plane. The AF component, which appears below $T_t=150$ K, has the same arrangement shown in YFe_xMn_{12-x} for $x=2$, 4, and 6. Above this temperature, all the moments are along *c* forming a ferromagnetic structure up to T_C. For YFe_8Mn_4, the Fe concentration (see Table I) is enough to favor an F coupling between the different sites and also to lead to the appearance of an F component in all the three 3*d* sublattices. This component is larger for the sites with higher Fe concentration (8*f* and 8*j* with $\theta=31°$ and 28° at 1.5 K), while in the site 8*i*, which is occupied mostly by Mn, the component is smaller along *c* ($\theta=60°$ at 1.5 K) than in the basal plane. This feature can be explained by the magnetocrystalline anisotropy of two types of sublattices that exist in YFe_8Mn_4: one is mostly occupied by Fe (8*f* and 8*j*) and the other by Mn (8*i*). In this way, the anisotropy of the Fe sublattices favors the *c* axis (being larger at high temperatures), while the anisotropy of the Mn sublattice favors the basal plane (being larger at low temperatures), in agreement with the magnetic behavior of YFe_xM_{12-x} (M=Ti, V, Mo, Si) compounds.

It is worth noting that the magnetic phase transition for YFe_8Mn_4, that takes place at $T_t=150$ K, does not correspond to an order-disorder (AF-para) phase transition, and therefore it is not appropriate to name this temperature the Néel temperature of the system, as it was quoted before.[9] Our interpretation of the neutron-diffraction data is more consistent with a canting of the magnetic moments from the *c* axis towards the basal plane below $T_t=150$ K. However, if a second-order parameter perpendicular to the spontaneous magnetization could be generated by higher-order exchange interactions (biquadractic, three-spin, and four-spin interactions), evidence for independent magnetic ordering along the *c* axis and in the basal plane would be observed. In order to elucidate these two possibilities, further research is needed investigating the third-order susceptibility.[39]

IV. MAGNETIC PHASE DIAGRAM

From the combined analysis of all the experimental data performed in the present work, we have established the magnetic phase diagram of YFe_xMn_{12-x} compounds (see Fig. 8).

YMn_{12} is an itinerant AF (AF-*I*, noncollinear magnetic moments in the basal plane favored by the Mn anisotropy)

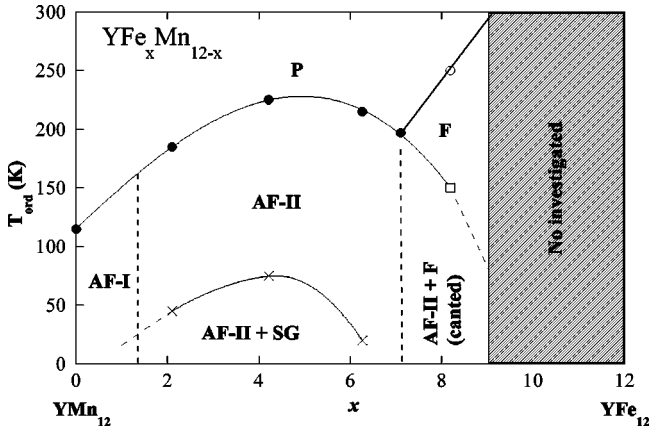

FIG. 8. Magnetic phase diagram of YFe_xMn_{12-x}. T_N(●) [the datum for $x=7$ has been taken from Morales *et al.* (Ref. 9)]; T_C(○); T_f(×); and T_t(□).

with reduced magnetic moments, small jump in C_p at the transition temperature, and spin fluctuations above T_N. The magnetic structure of YMn_{12} reflects already the site-selective dependence of the exchange interaction sign (Mn atoms at equal distances have F coupling if they are in sites $8f$ and AF coupling if they are in sites $8i$).

With the introduction of Fe, the extra electrons fill up the $3d$ Mn band leading to more localized states and giving rise to the increase of the magnetic moments, of the ordering temperature T_N, and of the jump in C_p at the transition temperature. In addition, the density of states at the Fermi level increases, being sufficient at $x=8$ for the appearance of ferromagnetism ($T_C=250$ K). In this compound, this ferromagnetism coexists at low temperatures with the same type of antiferromagnetism found for the compounds rich in Mn. It is expected that for higher x, the ferromagnetism will establish completely. In fact, our results for $TbFe_8Mn_4$ indicate that this AF component only remains in the site $8i$, being zero in all the other sites $8j$ and $8f$.[17]

YFe_xMn_{12-x} compounds with Fe concentration $x \leqslant 6$ are AF with the magnetic moments in the basal plane of the tetragonal structure, but the magnetic structure (AF-*II*) is different from the one of YMn_{12} (AF-*I*). There is a site dependence of the exchange interaction, regarding first neighbors: $8i$-$8i$ is AF, while at the same distance $8f$-$8f$ is F, and finally $8j$-$8f$ is AF in YMn_{12} but F for the compounds with $2 \leqslant x \leqslant 8$. In addition to these phases, a spin-glass behavior is observed at low temperatures for the compounds with $x=2,4,6$. This suggests that, as long as there is disorder, they are likely to exhibit spin-glass behavior. The disorder in these compounds is due to the dilution Fe/Mn and frustration of the competing exchange interactions, F (Fe) and AF (Mn), together with the different magnetic anisotropy of the two sublattices.

Regarding the magnetocrystalline anisotropy, the easy axis magnetization direction changes from the basal plane ($x<8$) to the c axis ($x=8$) of the tetragonal structure upon the addition of Fe, displaying the competition between the axial and planar anisotropies of the Fe and Mn sublattices, respectively. Below 150 K, in the F compound $x=8$ the planar anisotropy of the Mn sublattice overcomes the axial anisotropy of Fe, leading to a reorientation of the magnetic moments in the three crystallographic sites $8i$, $8j$, and $8f$ from the c axis to the basal plane, resulting in a canted magnetic structure.

V. CONCLUSIONS

In the present investigation, combining different physical properties of the body-centered-tetragonal YFe_xMn_{12-x} compounds, the magnetic phase diagram has been determined. Each phase and boundary have well been defined and characterized, and new phases have been evidenced. From these results, it seems that the interplay between competing exchange interactions and magnetocrystalline anisotropies in $3d$ sublattices mostly occupied by Mn (AF coupling and planar anisotropy) or Fe (F coupling and axial anisotropy) governs the physics of this system. This interplay makes the magnetism of these materials extremely sensitive to small changes in external parameters, such as temperature, magnetic field, or Fe concentration. In particular, the transfer of $3d$ Fe band electrons to the $3d$ Mn band seems to play a major role for understanding the crossover from antiferromagnetism to ferromagnetism, instead of the influence played by the distances between the $3d$ atoms and its neighbors, as was thought before.

ACKNOWLEDGMENTS

This work was supported by the projects No. MAT1999-0667-C04-03 and No. MAT2001-3507-C02-02 from MCYT and FEDER. We also thank the FCYT for the financial support given to E.A, and M. Artigas for the samples preparation.

*Also at: Universidad de Oviedo, Departamento de Física, Campus de Viesques, Edificio Este, 33203 Gijón, Spain. Email address: pique@epsig.uniovi.es; FAX: 34985182010.

[1] H. S. Li and J. M. D. Coey, in *Handbook of Magnetic Materials*, edited by K. H. J. Buschow (Elsevier, Amsterdam, 1991), Vol. 6.
[2] J. H. V. J. Brabers, V. H. M. Duijn, F. R. de Boer, and K. H. J. Buschow, J. Alloys Compd. **198**, 127 (1993).
[3] G. Venturini, B. Chafik El Idrissi, and B. Malaman, J. Magn. Magn. Mater. **94**, 35 (1991).
[4] S. H. Kilcoyne and M. T. Telling, J. Magn. Magn. Mater. **140**, 871 (1995).
[5] I. S. Dubenko, I. Yu. Gaidukova, Y. Hosokoshi, K. Inoue, and A. S. Markosyan, J. Magn. Magn. Mater. **195**, 687 (1999).
[6] J. Deportes and D. Givord, Solid State Commun. **19**, 845 (1976).
[7] Y. C. Yang, B. Kebe, W. J. James, J. Deportes, and W. Yelon, J. Appl. Phys. **52**, 2077 (1981).
[8] Y. Amako, S. Saoka, H. Yoshie, H. Nagai, and K. Adachi, J. Phys. Soc. Jpn. **64**, 1860 (1995).
[9] M. Morales, M. Bacmann, P. Wolfers, D. Fruchart, and B. Ouladdiaf, Phys. Rev. B **64**, 144426 (2001).
[10] J. B. Yang, W. B. Yelon, W. J. James, Q. S. Cai, D. Eckert, A. Handstein, K. H. Müller, and Y. C. Yang, Phys. Rev. B **65**, 064444 (2002).
[11] J. Stankiewicz, J. Bartolomé, and D. Fruchart, Phys. Rev. Lett. **89**, 106602 (2002).
[12] J. Stankiewicz, J. Bartolomé, and D. Fruchart, Phys. Rev. B **67**, 092409 (2003).
[13] R. J. Elliot and F. A. Wedgwood, Proc. Phys. Soc. London **84**, 63 (1964).
[14] J. Stankiewicz, J. Bartolomé, M. Morales, M. Bacmann, and D. Fruchart, J. Appl. Phys. **90**, 5632 (2001).
[15] E. Abad, Ph.D. Thesis, University of Oviedo, Spain (2001).
[16] J. Rodriguez-Carvajal, Physica B **192**, 55 (1993).
[17] C. Piqué *et al.* (unpublished).
[18] J. A. Blanco, J. C. Gómez Sal, J. Rodríguez Fernández, D. Gignoux, D. Schmitt, and J. Rodríguez Carvajal, J. Phys.: Con-

dens. Matter **4**, 8233 (1992).
[19] W. Zhang, E. M. Levin, and K. A. Gschneider, Jr., J. Magn. Magn. Mater. **250**, 170 (2002).
[20] Y. Elerman, S. Kervan, E. Duman, and M. Acet, J. Magn. Magn. Mater. **251**, 251 (2002).
[21] G. Hilscher, J. Magn. Magn. Mater. **27** 1 (1982).
[22] J. A. Mydosh, *Spin Glasses: An Experimental Introduction* (Taylor & Francis, London, 1993).
[23] J. J. Melero, Ph.D. Thesis, University of Zaragoza, Spain (1997).
[24] E. P. Wohlfarth, *Proprietés Magnetiques des Metaux et Alliages* (Grenoble, 1973).
[25] C. Piqué, R. Burriel, D. Fruchart, O. Isnard, and S. Miraglia, IEEE Trans. Magn. **30**, 604 (1994).
[26] F. Luis, P. Infante, J. Bartolomé, R. Burriel, C. Piqué, R. Ibarra, and K. H. J. Buschow, J. Magn. Magn. Mater. **140–144**, 1045 (1995).
[27] N. Okamoto, H. Nagata, H. Fujii, and W. Makihara, J. Magn. Magn. Mater. **70**, 139 (1987).
[28] R. Viswanathan and J. R. Clinton, in *Magnetism and Magnetic Materials–1974*, edited by C. D. Graham Jr., G. H. Lander, and J. J. Rhyne, AIP Conf. Proc. No. 24 (AIP, New York, 1975), p. 416.
[29] G. M. Kalvius, K.-H. Münch, A. Kratzer, R. Wäppling, D. R. Noakes, J. Deportes, and R. Ballou, Physica B **289–290** 261 (2000).
[30] T. Shinkoda, K. Kumagai, and K. Asayama, J. Phys. Soc. Jpn. **46**, 1754 (1979).
[31] H. Wada, H. Nakamura, E. Fukami, K. Yoshimura, M. Shiga, and Y. Nakamura, J. Magn. Magn. Mater. **70**, 17 (1987).
[32] I. H. Hagmusa, J. C. P. Klaasse, E. Brück, F. R. de Boer, and K. H. J. Buschow, J. Alloys Compd. **297**, 21 (2000).
[33] R. J. Graves Tompson and H. W. White, J. Appl. Phys. **54**, 2838 (1983).
[34] K. Yoshimura, H. Yasuoka, and Y. Nakamura, J. Magn. Magn. Mater. **90-91**, 706 (1990).
[35] A. Hernando, J. M. Rojo, J. C. Gómez Sal, and J. M. Novo, J. Appl. Phys. **79**, 4815 (1996).
[36] M. Morales, M. Bacmann, Ch. Baudelet, A. Delobbe, D. Fruchart, Ch. Giorgetti, G. Krill, and P. Wolfers, J. Alloys Compd. **317-318**, 470 (2001).
[37] G. Hilscher and H. Kirchmayr, J. Phys. (Paris), Colloq. **40**, C5-196 (1979).
[38] K. Hardman-Rhyne and J. J. Rhyne, J. Less-Common Met. **94**, 23 (1983).
[39] U. Köbler, R. M. Mueller, W. Schnelle, and K. Fischer, J. Magn. Magn. Mater. **188**, 333 (1998).